Journal of
Applied Crystallography
ISSN 0021-8898
Editor: **Anke R. Pyzalla**

Direct mapping of fiber diffraction patterns into reciprocal space

Norbert Stribeck and Ulrich Nöchel

J. Appl. Cryst. (2009). **42**, 295–301

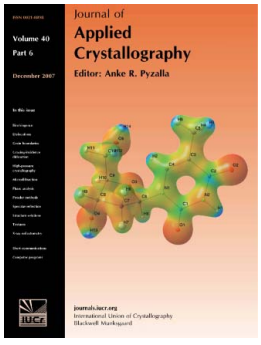

Journal of
Applied Crystallography
ISSN 0021-8898

Received 23 September 2008
Accepted 9 February 2009

Direct mapping of fiber diffraction patterns into reciprocal space

Norbert Stribeck* and Ulrich Nöchel

Institute of Technical and Macromolecular Chemistry, Department of Chemistry, University of Hamburg, Bundesstrasse 45, 20146 Hamburg, Germany. Correspondence e-mail: norbert@stribeck.de

On the basis of the concept of Polanyi [*Z. Phys.* (1921), **7**, 149–180], the mapping of fiber diffraction patterns into reciprocal space is revisited. The result is a set of concise mapping relations that does not contain any approximations. This set permits the design of a direct method that, in principle, does not require refinement of mapping parameters even for patterns of tilted fibers. The method is unsuitable for diffuse scattering patterns. If inaccuracies of two pixels can be tolerated, a pattern is automatically mapped into reciprocal space in real time. The method is proposed for the processing of the extensive sets of patterns that are recorded in time-resolved wide-angle X-ray diffraction investigations of polymer materials.

1. Introduction

Fiber diffraction patterns must be mapped into reciprocal space before they can be analyzed quantitatively. For this purpose, interactive computer programs are utilized that rest upon unnecessary (Stribeck, 2009) approximations (Rajkumar *et al.*, 2005; Bian *et al.*, 2006). Such a design is no disadvantage in crystallography, because sophisticated interactive refinement methods are required anyway for the exact determination of crystal structure parameters.

In contrast, in materials science, time-resolved experiments are frequently carried out, and voluminous series of diffraction patterns must be processed. Here the crystal structure parameters are already known, in general. Thus, minor inaccuracy of the mapping can be tolerated, if variation of peak intensity or shape is monitored. In this case it is important to carry out the mapping quickly and automatically. Because the fiber tilt may change during the experiment, the algorithm must be able to track and to compensate such variation. Thus, revisiting the theoretical treatment of fiber mapping appears promising. This has been demonstrated in a recent paper (Stribeck, 2009) by showing that there is no principal reason to refine an approximate center of the fiber pattern iteratively. Moreover, instead of an approximation (Franklin & Gosling, 1953; Fraser *et al.*, 1976) of the tilt angle β of the fiber (with respect to the normal plane to the X-ray beam), the recently deduced (Stribeck, 2009) exact equation is employed. In the present work an algorithm is presented by which the mapping can be performed quickly and automatically. Its design rests on application of the aforementioned findings. Intricate parametrization is simplified, and slow trigonometric functions are avoided to a large extent. Methods of digital image processing facilitate circumvention of time-consuming case statements. Finally, the theoretical consideration results in the determination of a constant factor that had remained undetermined in the treatment of Fraser *et al.* (1976).

2. Geometrical mapping from the plane detector into reciprocal space

Let a planar detector be placed at a distance R from the fiber sample. Let $C(\mathbf{p})$ be the number of counts recorded on the detector in the pixel at the position $\mathbf{p} = (p_1, p_3)$ of area $\mathrm{d}p_1\,\mathrm{d}p_3$. Then $I(\mathbf{p}) = C(\mathbf{p})/(\mathrm{d}p_1\,\mathrm{d}p_3)$ is the scattering intensity. The aim is to determine the mapping of the scattering intensity $I(\mathbf{p}) \rightarrow I(\mathbf{s})$ into reciprocal space $\mathbf{s} = (s_{12}, s_3)$ with fiber symmetry. $s_{12} = (s_1^2 + s_2^2)^{1/2}$ is the equatorial and s_3 the meridional component of the scattering vector. Its modulus is defined as

$$|\mathbf{s}| = s = (2/\lambda)\sin\theta. \tag{1}$$

Here λ is the wavelength of the radiation and 2θ is the scattering angle.

The relations that map the image of the untilted fiber from the detector plane into reciprocal space are readily established:

$$s_1 = \frac{1}{\lambda}\frac{p_1}{(R^2 + p_1^2 + p_3^2)^{1/2}}, \tag{2}$$

$$s_2 = \frac{1}{\lambda}\left[\frac{R}{(R^2 + p_1^2 + p_3^2)^{1/2}} - 1\right], \tag{3}$$

$$s_3 = \frac{1}{\lambda}\frac{p_3}{(R^2 + p_1^2 + p_3^2)^{1/2}}, \tag{4}$$

and fiber tilt is considered by subjecting equations (2)–(4) to the rotation (Lorenz & Holmes, 1993)

$$\mathbf{D}(\beta) = \begin{pmatrix} 1 & 0 & 0 \\ 0 & \cos\beta & -\sin\beta \\ 0 & \sin\beta & \cos\beta \end{pmatrix}. \qquad (5)$$

These forward mapping relations $\mathbf{p} \rightarrow \mathbf{s}$ can be used to visualize the principal properties of the fiber mapping (Fig. 1).

Nevertheless, they are of little practical value, because employing them in a mapping algorithm results in an incomplete **s** map (with scattered holes). Consequently, it makes sense to invert the process by stepping through a predefined **s** map, thus making sure that the result is contiguous. For this purpose, the equations of the reverse mapping must be deduced, and this requires sophisticated geometrical abstraction of the problem.

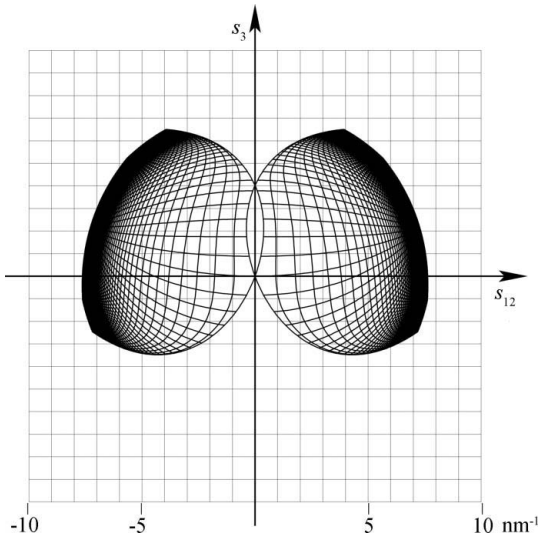

Figure 1
Grid map of the detector plane (p_1, p_3) as mapped into reciprocal space (s_{12}, s_3) for a grid with $\Delta p = 1$ cm, a fiber tilt of $\beta = 20°$, wavelength $\lambda = 0.15$ nm and a sample-to-detector distance $R = 7$ cm.

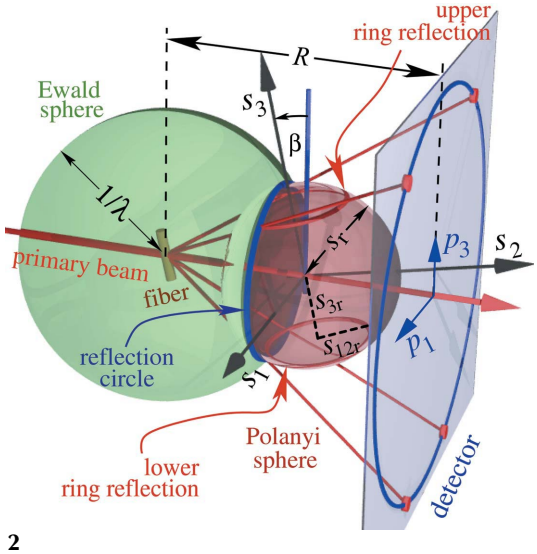

Figure 2
Sketch of fiber diffraction geometry with the Ewald sphere and a Polanyi sphere. The intersection is a circle ('reflection circle') that does not change as the fiber is tilted (tilt angle β). The radius of the Polanyi sphere is chosen to match the magnitude s_r of a model ideal reflection manifested in two rings $(s_{12r}, \pm s_{3r})$. The trihedron (s_1, s_2, s_3) indicates reciprocal space. R is the distance between fiber and detector. (p_1, p_3) indicates the detector coordinate system.

2.1. Geometrical relations

According to Polanyi (1921), the geometry of fiber diffraction is advantageously described in terms of reflection circles. Such circles are the intersections of the Ewald sphere with Polanyi spheres of varying diameter (Fig. 2).

If the tilt angle β of the fiber is varied in an experiment, the image spots of the ring reflections move – each on its own reflection ring – but noticeable intensity variation is not observed on the detector, as long as the spots do not disappear at the meridian. As sketched in Fig. 2, central projection maps the spots in reciprocal space onto the detector placed at a distance R from the fiber. Thus, it is advantageous to use plane polar coordinates with the meridian as the reference direction for the parametrization of the functions $C(\mathbf{p})$ and $C(\mathbf{s})$. Considering the pulses $C(p, \delta)$ accumulated in the pixel on the detector that is found on the reflection circle of radius p under the direction angle δ with respect to the meridian, the aim is to find the reverse mapping $C(s, \rho) \rightarrow C(p, \delta)$ of the pixel from reciprocal space onto the detector plane. In **s** space the pixel is located on the reflection circle of radius s under the direction angle ρ. Taking the meridian s_3 as the reference axis let $\cos\rho = s_3/s$. Analogously, on the detector $\cos\delta = p_3/p$ is defined. The relation of this Polanyi (1921) parametrization to the common parametrization on the Ewald sphere is sketched in Fig. 3.

Because the radius s is already defined by the scattering angle 2θ [*cf.* equation (1)] Polanyi (1921) only adds the direction angle δ, whereas the authors of later papers on fiber mapping (Fraser *et al.*, 1976; Millane & Arnott, 1985) split the scattering angle 2θ into its latitude χ and longitude μ. Anticipating a simplification in our algorithm, it is worth noting that χ, μ and 2θ form a right spherical triangle, and thus

$$\cos\mu\cos\chi = \cos 2\theta. \qquad (6)$$

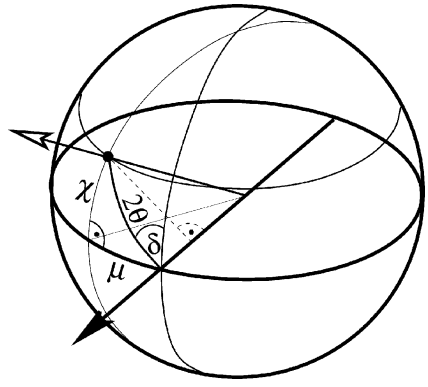

Figure 3
Two parametrizations for the direction of the diffracted beam (open arrow head, diffraction angle 2θ). Polanyi (1921) only adds the direction angle δ. In the customary method (Fraser *et al.*, 1976; Millane & Arnott, 1985) the direction is parametrized by latitude χ and longitude μ on the Ewald sphere.

2.2. The central projection of the reflection circles

The reflection circle in **s** space is the intersection of the Ewald sphere and a Polanyi sphere. From Fig. 2, it is deduced that the distance between the sample and the reflection circle is

$$\ell_1 = \frac{1}{\lambda} - \frac{\lambda}{2}s^2 = \frac{2-\lambda^2 s^2}{2\lambda} = \frac{\cos 2\theta}{\lambda}. \tag{7}$$

The radius r_c of this circle is $r_c = s\cos\theta$, *i.e.* r_c is (*cf.* Fig. 3, dashed line) the height of the triangle in the Ewald sphere that is formed by the primary beam, the diffracted beam and the scattering vector **s**. The circle of radius r_c is mapped onto a circle of radius p in the plane of the detector. The theorem of intersecting lines yields

$$r_c/p = \ell_1/R. \tag{8}$$

Moreover, from trivial scattering geometry

$$p = R\tan 2\theta. \tag{9}$$

For the computation, use of the slow tangent function can be avoided. First, the identity $\tan 2\theta = 2\tan\theta/(1-\tan^2\theta)$ reduces the angle, and the definition of the scattering vector yields $\tan\theta = \lambda s/[2(1-\lambda^2 s^2/4)^{1/2}]$. As an intermediate result of tilt-angle computation (Stribeck, 2009), the distance R is readily determined. Thus, on the detector the pixels on the reflection-circle image are easily accessed, and with equation (8) the first of two reverse mapping relations

$$p(s) = \frac{2\lambda R s}{2-\lambda^2 s^2}\left(1-\frac{\lambda^2 s^2}{4}\right)^{1/2} = \frac{\lambda R s}{\cos 2\theta}\cos\theta \tag{10}$$

is established. It describes the radial component of the reverse mapping.

2.3. The direction angles in the reflection circles

Polanyi's equation (Polanyi, 1921; Stribeck, 2009)

$$\cos\delta = \frac{\cos\rho - \sin\theta\sin\beta}{\cos\theta\cos\beta} \tag{11}$$

describes the azimuthal aspect of the reverse fiber mapping. Similar to equation (6) the Polanyi equation is established from a spherical triangle, but on the Polanyi sphere.

Consider in Cartesian coordinates a point in reciprocal space (s_{12}, s_3) with $s^2 = s_{12}^2 + s_3^2$. Let (p_1, p_3) be the corresponding position on the detector, then

$$p_3(s_{12}, s_3) = \frac{2\lambda R s}{2-\lambda^2 s^2}\,\frac{s_3/s - (\lambda s/2)\sin\beta}{\cos\beta} \tag{12}$$

follows from simple substitution in equation (11). Additionally taking into account the radial mapping relation equation (10) and $p_1 = (p^2 - p_3^2)^{1/2}$,

$$p_1(s_{12}, s_3) = \frac{2\lambda R s}{2-\lambda^2 s^2}\left\{1-\frac{\lambda^2 s^2}{4} - \left[\frac{s_3/s - (\lambda s/2)\sin\beta}{\cos\beta}\right]^2\right\}^{1/2} \tag{13}$$

is obtained for the horizontal position of the pixel on the detector.

It is well known (Fraser *et al.*, 1976; Stribeck, 2007) that not every pixel (s_{12}, s_3) in the range of the fiber mapping will have information in its domain (p_1, p_3) on the detector – the fiber mapping is not surjective (*cf.* Fig. 1). The position and size of the remnant blind areas are a function of the tilt angle β. Blind areas are bordered by circles of radius $1/\lambda$ (*i.e.* the radius of the Ewald sphere). Actually, on the meridian there are only two points that can be mapped. These are the origin and the pixel at $(0, s_{3\beta})$ with $s_{3\beta} = (2/\lambda)\sin\beta$. Thus, the centers of the bordering circles are at $s_{1c} = \pm(1/\lambda^2 - s_{3\beta}^2/4)^{1/2}$ and $s_{3c} = s_{3\beta}/2$. On the left side of the reciprocal space map only the *interior* of the left circle and the *exterior* of the right circle are found on the detector. On the right side of the map it is the other way round. In classical programming languages the test for a blind pixel is accomplished by complex and time consuming `if` statements (Fraser *et al.*, 1976). In a matrix processing language [PV-WAVE (VNI, 2007), IDL (RSI, 2004) or MATLAB (The Mathworks Inc., Natick, MA, USA)] this construct can be circumvented. For this purpose a grid map of reciprocal space is filled by ones, and the circular blind areas are set to zero by application of the library function DIST (distance from a center) that is a corner stone of digital Fourier transformation. The result is a map `validmask`, in which only the transformable pixels are set to 1. After that the mapping is accomplished by fast matrix processing statements. In PV-WAVE the two statements

```
; make point list
pl = WHERE (validmask)
recip.map(pl) = detec.map(p1map(pl), p3map(pl))
```

perform the geometrical transformation, after the matrices `p1map` and `p3map` have been computed according to equations (13) and (12).

3. Intensity mapping

Intensity mapping is the correction of the function value after geometrical mapping. The counts recorded in pixels of constant size on the detector are distributed in reciprocal space on elements of varying area and the intensity (counts per area) is changed. This intensity change is considered (Fraser *et al.*, 1976) by multiplication with the value of the Jacobian determinant J_F of the reverse fiber mapping, $\mathbf{p}(\mathbf{s})$, at the position **s** of the considered pixel.

According to observation during fiber tilting experiments, the reflection spots are moving on their reflection circles without noticeable intensity change. Thus, only the central projection of the reflection circles is making it into the Jacobian, whereas the azimuthal component of the fiber mapping according to equation (11) is not considered. In fact, this suggestion is an implied premise of the result

$$J_F = \frac{K R^2}{\cos^3 2\theta} = \frac{K R^2}{(1-\lambda^2 s^2/2)^3} \tag{14}$$

presented by Fraser *et al.* (1976). Here K is a constant, and we have simplified the denominator using equation (6). This proposition shall now be made plausible by discussion of the

complete Jacobian J_C. It appears advantageous to start from equations (10) and (11) in polar coordinates and to compute

$$J_p = \left| \frac{\partial p}{\partial s} \frac{\partial \delta}{\partial \rho} - \frac{\partial p}{\partial \rho} \frac{\partial \delta}{\partial s} \right| = \frac{dp}{ds} \frac{\partial \delta}{\partial \rho}, \tag{15}$$

taking into account that $p(s)$ is no function of the direction angle ρ. Because the detector pixels are addressed in Cartesian coordinates, angle increments are replaced by arc lengths

$$J_C = \frac{dp}{ds} \frac{p}{s} \frac{\partial \delta}{\partial \rho}, \tag{16}$$

and the required Jacobian for the complete fiber mapping is obtained. From equation (10) it follows that

$$\frac{dp}{ds} = \frac{\lambda R}{\cos^2 2\theta \cos \theta}. \tag{17}$$

Partially deriving equation (11) one obtains

$$\frac{\partial \delta}{\partial \rho} = \frac{1}{\cos \theta \cos \beta} \frac{\sin \rho}{\sin \delta}, \tag{18}$$

and with equation (10) the result is

$$J_C = \frac{\lambda^2 R^2}{\cos^3 2\theta} \frac{\partial \delta}{\partial \rho}. \tag{19}$$

Comparison with equation (14) yields $K = \lambda^2$ for the constant of Fraser *et al.* (1976). In Cartesian coordinates,

$$J_C = \left| \frac{\partial p_1}{\partial s_{12}} \frac{\partial p_3}{\partial s_3} - \frac{\partial p_1}{\partial s_3} \frac{\partial p_3}{\partial s_{12}} \right|, \tag{20}$$

equations (12) and (13) return the same result with

$$\frac{\partial \delta}{\partial \rho} = \frac{|s_{12}|}{(\lambda s^2 s_3 \sin \beta + s_{12}^2 \cos^2 \beta - s_3^2 \sin^2 \beta - \lambda^2 s^4/4)^{1/2}} \tag{21}$$

after more involved computation. As mentioned above, it is suggested to neglect this term. At the outer edge of the detector $\partial \delta / \partial \rho \simeq 1$ is negligible anyway, but shows a singularity along the meridian of the detector plane. We believe the reason that, in general, it should be neglected is twofold. First, it does not consider the smearing of the measured scattering intensity by the primary beam profile. Second, it describes the mapping in a mathematically ideal plane-to-plane mapping but does not consider the cylindrical symmetry of the fiber pattern in reciprocal space. The term $\partial \delta / \partial \rho$ compensates the projection onto the detector plane of a hypothetical infinitesimally thin pixel from which the intensity is supposed to emanate. This pixel does not lie flat on the surface of the Ewald sphere but is on a central slice through Polanyi's sphere, *i.e.* on the plane that is formed by the position of the considered pixel on the Polanyi sphere and its axis. By putting these pixel tiles side by side on a level surface, a grid image of the fiber plane (s_{12}, s_3) is obtained (plane-to-plane mapping).

In the projection compensation accomplished by $\partial \delta / \partial \rho$ [equation (18)], the sub-term $(\cos \theta \cos \beta)^{-1}$ considers the orientation of the Polanyi sphere, and $\sin \rho / \sin \delta$ considers the actual orientation of the central slice of the Polanyi sphere to which the hypothetical pixel tile is attached. Whenever the hypothetical pixels are at the meridian, their projection onto the detector plane vanishes. In the term $\partial \delta / \partial \rho$ this is 'compensated' by the aforementioned singularity. Nevertheless, in reality the intensity counted in a detector pixel emanates not from an infinitesimally thin plane pixel but from a small volume in reciprocal space owing to the smearing of the ideal intensity function with the primary beam profile. Because the detector pixel is probing a small volume, it probes a region of constant intensity that is distributed on a reflection ring (*cf.* Fig. 2). Consequently it does not matter from which direction this small *volume* light-source is viewed – its intensity appears to be the same. Thus, we agree that the intensity correction of the real fiber mapping is accomplished by only

$$J_F = \frac{\lambda^2 R^2}{\cos^3 2\theta} = \frac{\lambda^2 R^2}{(1 - \lambda^2 s^2/2)^3}. \tag{22}$$

In PV-WAVE the corresponding code is

```
; Build the Jacobian for intensity correction
cos2thetamap = 1.0 - (lambda * smap)^2/2
jacmap = (lambda * samp) ^2/cos2thetamap^3
; Correct the intensity
recip.map = recip.map * jacmap * absmap * polmap
```

It is carried out after the geometrical mapping. All `maps` are matrices. `jacmap` is the Jacobian. `absmap` is the well known map for absorption correction and `polmap` implements the polarization correction (Stribeck, 2007).

4. Example

An example demonstrates the direct fiber mapping by the procedures `wf_premap` and `wf_map` written in PV-WAVE (VNI, 2007). The commented source code is available (Stribeck, 2008).

After the setup of the X-ray beamline, the alignment of the plane detector with respect to the primary beam has to be checked. For this purpose the diffraction pattern of an isotropic crystalline sample is recorded. For example, the Debye–Scherrer rings of a tripalmitate sample are not ellipses, but perfect circles. With proper alignment, it is unnecessary to correct the pattern for a tilted detector plane. Similarly, it is unnecessary to determine the sample-to-detector distance R from the calibration pattern, as long as the experiments are carried out on materials with sharp reflections that can be used as internal standards.

4.1. Determination of data required by the pre-mapping and mapping procedures

For each series of diffraction patterns from a time-resolved experiment, some mapping parameters must be determined once interactively. Thereafter patterns can be mapped automatically. Our procedure `wf_premap` assumes that the studied material exhibits a sharp reflection that is located neither on the equator nor on the meridian. In the example we investigate polypropylene and select the 131 reflection of the crystallographic α_2 modification as the internal standard. With the crystallographic c axis parallel to the meridian, the reflection is characterized by the parameters (Mencik, 1972) $d_{hk\ell} = d_{131} =$

0.406 nm, which defines the diameter of its Polanyi sphere, and $c/\ell = 0.6504$ nm, which defines the position of the reflection ring on this sphere. The wavelength of X-radiation (here $\lambda = 0.15$ nm) must also be known. In this case the first pre-mapping run of the series is started by

```
wave>ab = wf_premap (ss, a, 0.15, 0.406, 0.6504)
```

Entering the numbers in ångström units yields an **s** map scaled in inverse ångström, instead. The procedure requires a diffraction pattern as input (`a`). It generates output both in a 'save-set' (`ss`) and in a background-corrected diffraction pattern (`ab`). If the provided save-set is still empty, the procedure enters interactive mode and the user is presented the pattern as shown in Fig. 4. This pattern is already corrected for inclined background. For this purpose the procedure has determined an almost planar background by spatial frequency filtering, has subtracted it and has added the average value of this background.

Obviously, in Fig. 4 the meridian is not vertical and the fiber is tilted. By means of the pointing device the user draws the reflection circle through the maxima of the reflection spots of the 131 reflection. Thereafter the user transforms the circle into a belt that is wide enough to contain the maxima of the spots (Fig. 4).

Now the procedure cuts out this belt and presents it to the user, who finally specifies four disjoint clips (regions of interest on the reflection circle). This is achieved by punching out circular regions from the belt (one is indicated in red in Fig. 4). The clips are the intersections of the belt (white double band) and the (red) circles. They may be chosen rather long. It is only required that the absolute maximum inside the clip is the maximum of a unique reflection spot for all diffraction patterns recorded during the experiment. The program sorts the four clips assuming that the meridian is between the two highest ones and determines the positions of the maxima in the clips. From these four maximum positions the best reflection circle is determined by regression. The error of determination is computed. In general, it is below one pixel. Subsequently, the orientation of the meridian is computed both from the upper and from the lower pair of spots. The difference is, in general, approximately 0.1°. On the basis of this information the diffraction pattern is centered and aligned. Finally, the program computes the tilt angle β of the fiber from the orientation angles δ and δ' of the spots using the exact equation

$$\tan\beta = \left[(4 - \lambda^2 s_r^2)^{1/2}/2\lambda s_r\right](\cos\delta' - \cos\delta) \qquad (23)$$

derived by Stribeck (2009). Here $s_r = 1/d_{131}$ is the radius of the Polanyi sphere of the reference 131 reflection. Finally, the save-set `ss` is filled with a set of data: the tilt angle β; the true radius p_r of the reference-reflection circle on the detector; the crystallographic data of the reference reflection; the wavelength λ; and the geometrical data of the four clips. This information is sufficient for an automatic processing of the complete series of diffraction patterns recorded in a time-resolved X-ray diffraction experiment of materials with fiber symmetry.

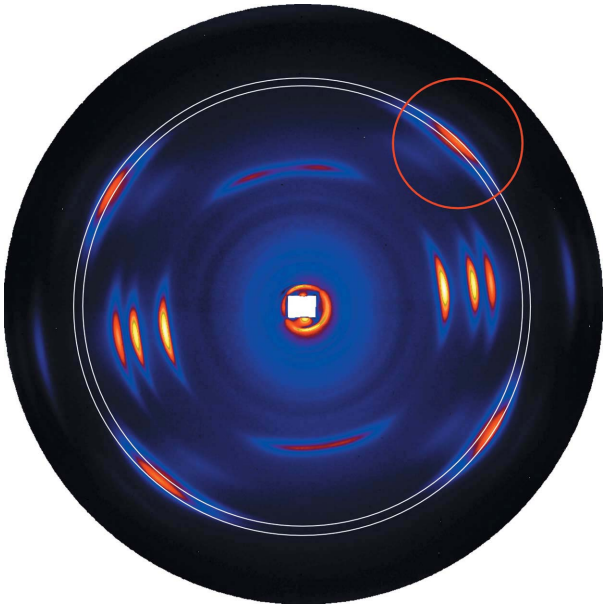

Figure 4
Interactive mode of `wf_premap`. Draw the reflection circle through the centers of the reflection spots of an internal standard reflection (here the polypropylene 131 reflection), and widen the circle into a belt that contains the maxima of the reflection spots. Finally input four circles (one indicated in red).

4.2. Automatic mapping

If the procedure `wf_premap` is called with a filled save-set, the interactive part is skipped, and the geometry of the four clips is taken from the save-set. The positions of the spot maxima are computed, and the image is centered and aligned. If the sample is melting and the reflections become too weak, `wf_premap` can be called with the keyword `/keep` to switch off tracking of the mapping parameters. A typical result is shown in Fig. 5.

Finally, the mapping into reciprocal space is accomplished by the routine `wf_map`. The routine first determines a suitable size of the map in **s** space from the size of the pattern in detector space. The **s**-space map is set up with an equidistant grid. The distance R measured in pixel units is computed from p_r by means of equation (9). As explained in the theoretical part, the mask `validmask` is generated. Then the mapping into reciprocal space is accomplished by a few elementary matrix operations. The call

```
wave>rec = wf_map (ss, ab)
```

maps the diffraction pattern `ab` under consideration of `ss` into the pattern `rec` in reciprocal space. For the purpose of a study in the field of applied materials science, the resulting tilt angle appears to be sufficiently accurate, in general. Nevertheless, manual refinements can be accomplished by calling the procedure with a different parameter list, *e.g.*

```
wave>rec = wf_map (ss, ab, /show, 10.5)
```

Then the mapping is carried out with the user-supplied tilt angle of 10.5°, and after finishing, the diffraction pattern is

shown on a polar grid that permits an assessment of the remnant distortion. Fig. 6 shows a typical result obtained by automatic direct mapping.

In the example, the computed tilt angle is $\beta = 5.85^\circ$. Because the resulting pattern is in reciprocal space, it should exhibit symmetry in four quadrants. Thus, the quality of the mapping can be assessed by comparison with a four-quadrant average of the pattern. The four-quadrant average example pattern is shown in Fig. 7.

The averaged pattern looks very similar to the pattern returned by `wf_map`. Nevertheless, in the arc reflections of the averaged pattern that are close to the meridian some mismatch of up to two pixels is observed due to inaccuracy of the direct mapping.

5. Conclusion

The relations for the mapping of a fiber diffraction pattern onto a plane detector have been simplified by geometrical analysis. The presented direct algorithm for the reverse mapping exploits the results of these considerations. It is designed for the processing of the extensive data sets that result from experiments in materials science, in which the reaction of oriented semicrystalline polymer materials upon cycling of load or temperature is monitored by wide-angle X-ray scattering. By means of the direct method we are able to process 1000 patterns per day. The accuracy of the direct method is lower than that of interactive refinement procedures. Nevertheless, it appears sufficient for the determination of integral reflection intensities and for the study of integral breadths.

Application is demonstrated in a follow-up paper (Stribeck *et al.*, 2009) focusing on the quantitative analysis. For the determination of a total reflection intensity, fiber scattering is integrated with respect to rotation about the fiber axis, the reflection is separated from its background and the integral is computed. Integral breadths can be determined after projecting the separated peak onto the radial or the azimuthal direction. Thus, information on crystal size or orientation distribution is obtained (Stribeck *et al.*, 2009). The processes of the filling of the meridional gap by two-dimensional extrapolation and the separation of the peak from its background are, however, still time consuming. For this reason the time requirement even for automatic analysis increases beyond the time spent on the experiment. Moreover, the result becomes inaccurate as the peaks become weak or parts of the peaks become inaccessible because they are hidden in the meridional gap of fiber scattering. The hidden peak fraction may even vary, as a melting fiber may bend during the experiment.

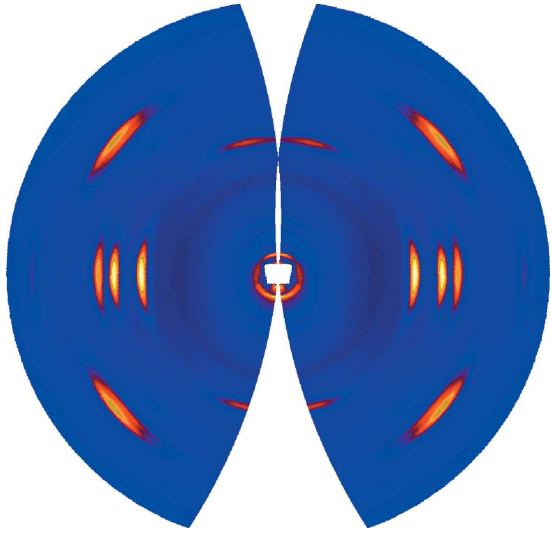

Figure 6
The procedure `wf_map` has mapped the fiber diffraction pattern into reciprocal space

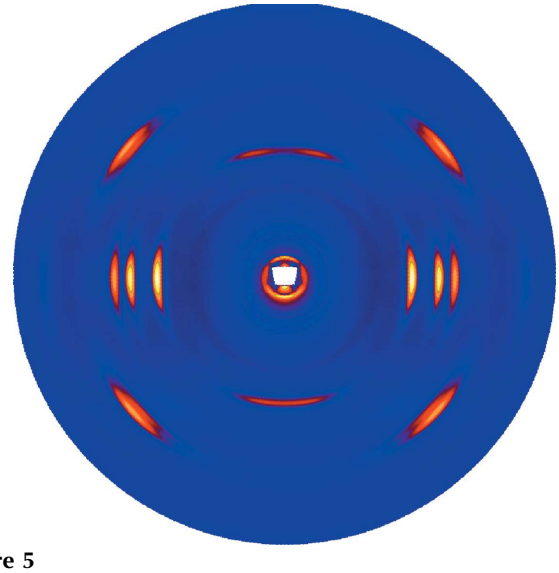

Figure 5
After pre-mapping the image is centered and aligned. The tilt angle β has been determined but not yet considered

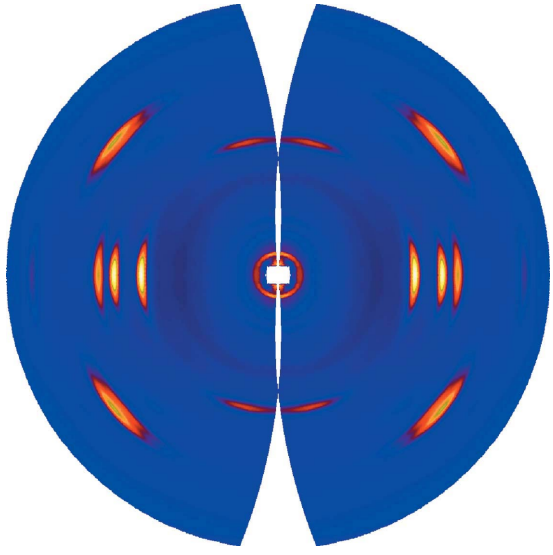

Figure 7
A four-quadrant average of the fiber pattern mapped into reciprocal space shows little difference as compared with the direct result of the mapping. Nevertheless, at the borders of overlapping valid regions some jitter is noticed

Such bending may be overlooked or misinterpreted if the fiber pattern is not mapped but interpreted directly. Despite the addressed difficulties we estimate that the quantitative analysis of fiber patterns has the potential to increase the level of knowledge on structure evolution in fibers. Direct fiber mapping may be a first step on this path.

For the determination of crystallographic data, on the other hand, it will remain necessary to refine mapping parameters by means of the computer programs that are specially designed for this purpose. Moreover, if samples with more diffuse scattering patterns are to be studied it may become impossible to determine the mapping parameters by an internal standard. In this case the described pathway for an automatic mapping is not viable.

The authors thank the Hamburg Synchrotron Radiation Laboratory (HASYLAB) for beam time granted under project No. II-04-039. We gratefully acknowledge funding by the Deutsche Forschungsgemeinschaft, project STR 501/4-2. Part of this work has been supported by the 7th Framework Programme of the European Union (project 213436 NANO-TOUGH).

References

Bian, W., Wang, H., McCullough, I. & Stubbs, G. (2006). *J. Appl. Cryst.* **39**, 752–756.
Franklin, R. E. & Gosling, R. G. (1953). *Acta Cryst.* **6**, 678–685.
Fraser, R. D. B., Macrae, T. P., Miller, A. & Rowlands, R. J. (1976). *J. Appl. Cryst.* **9**, 81–94.
Lorenz, M. & Holmes, K. C. (1993). *J. Appl. Cryst.* **26**, 82–91.
Mencik, Z. (1972). *J. Macromol. Sci. Part B Phys.* **6**, 101–115.
Millane, R. P. & Arnott, S. (1985). *J. Macromol. Sci. Part B Phys.* **24**, 193–227.
Polanyi, M. (1921). *Z. Phys.* **7**, 149–180.
Rajkumar, G., Al-Khayat, H., Eakins, F., He, A., Knupp, C. & Squire, J. (2005). *Fibre Diffr. Rev.* **13**, 11–18.
RSI (2004). Interactive Data Language, IDL. Version 6.1. Research Systems Inc., Boulder, Colorado, USA.
Stribeck, N. (2007). *X-ray Scattering of Soft Matter.* Heidelberg, New York: Springer.
Stribeck, N. (2008). http://www.chemie.uni-hamburg.de/tmc/stribeck/dl.
Stribeck, N. (2009). *Acta Cryst.* A**65**, 46–47.
Stribeck, N., Nöchel, U. & Funari, S. S. (2009). *Macromolecules*. In the press.
VNI (2007). *PV-WAVE Manuals*. Version 7.5. Visual Numerics Inc., Houston, Texas, USA.